Using SED Model Fitting to Search for Star-Forming Galaxies at $z > 4.5$

Catherine Slaughter

1. INTRODUCTION

Active Galactic Nuclei (AGN) sit at the center of galaxies. They are super massive black holes (SMBH) with an accretion disk of material from their host galaxies. The process of accretion is incredibly efficient, and as such, AGNs are extremely luminous, able to completely outshine their host galaxies in some cases. AGNs are a significant topic of current research. They're visible in a wide range of the EM spectrum, not super well understood, and may be able to shed more light on galaxy formation processes. Cowie et al. (2020) aims to learn more about the formation and early evolution of AGNs. We have large samples of spectroscopically confirmed AGNs in areas of redshift z=1-5, but the number of AGNs spectroscopically identified at redshifts $z > 5.5$ only number a few hundred (see Fig. 1), and of these, only a few tens have been successfully observed in X-ray. These are some of the most luminous AGNs in the population. The Chandra Deep Field (CDF) north and south images can potentially observe much fainter X-ray sources, but only one additional $z > 5$ spectroscopically confirmed AGN has been found from these.

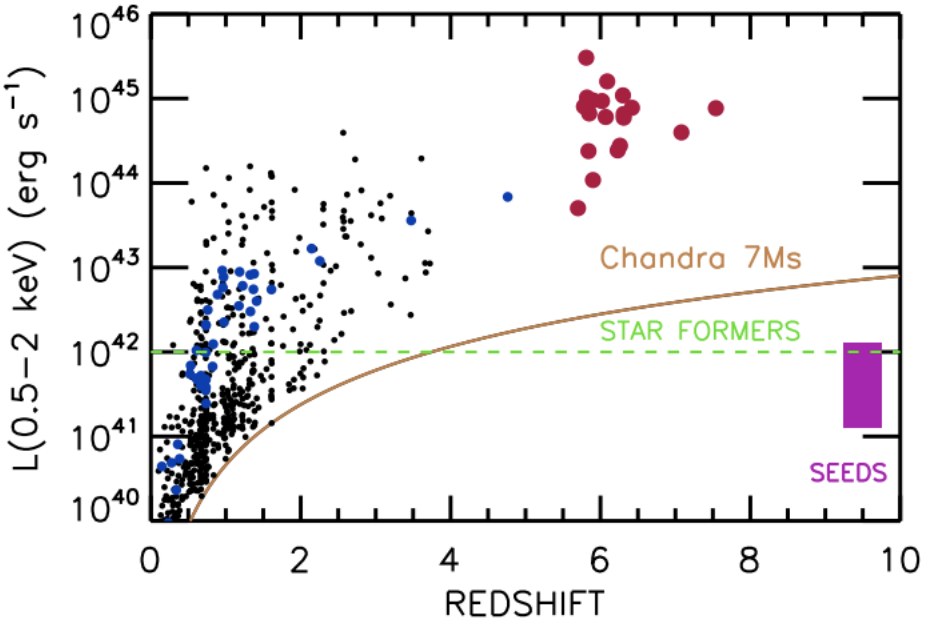

Figure 1. Luminosity vs redshift for sources of interest. The gold curve shows the limit for Chandra, and the green dotted line represents the luminosity below which the X-ray contribution of star formation in the host galaxy becomes relevant. Spectroscopically-identified sources from CDF-S are plotted in black. While X-ray detected sources of redshift $z > 5.5$ are shown in red. Additionally, the purple box represents a possible range of $10^4 - 10^4 M_\odot$ direct-collapse SMBH seeds

This is strange, because the area from $z = 5 - 10$ is considered to be a time of growth in the seeds of SMBHs. The seeds of these SMBHs, most likely Population III stellar remnants or direct-collapse black holes, exist at redshifts $z > 10$. Cowie et al. (2020) looks to determine whether there really was little SMBH growth in the $z = 5 - 10$ period, or if there is simply too small s number of very luminous sources to see. They conclude the former, that there are too few high-redshift AGN sources to account for SMBH growth during this time. In particular, the paper notes a distinct drop in AGN number density from $3 < z < 6$.

2. ASTROPHYSICAL CONCEPTS

There's a lot in this paper that is related to topics learned in class this term. we learned in class that looking further out (higher z) allows us to see what the universe looked like at an earlier time. This understanding is crucial to the conclusions of Cowie et al. (2020). We have also learned about AGN structure. In class, we learned that different parts of an AGN emit different wavelengths of light, so its easy to study a specific structure of an AGN simply by looking in the correct frequency. This knowledge is crucial to my extended analysis, which looks at spectral energy shapes. This paper also seeks to observe possible AGN sources in the X-ray, near/mid IR, and submillimeter regions of the electromagnetic spectrum. Near the end of term, we learned how photometric redshift is calculated using the Lyman-α 912-angstrom break. This process is how Cowie et al. (2020) calculates redshift, because the distance to these sources makes it difficult to measure spectra.

3. METHODS

The primary purpose of Cowie et al. (2020) was to search for high-redshift AGN in the Chandra Deep Field South (CDF-S). It is remarkably difficult to directly observe objects that are so far away, so they conducted their search in a number of ordered steps.

To start, Cowie et al. (2020) looked for direct detection X-ray AGN sources, that had previously calculated photometric redshifts greater than 4.5. As mentioned previously, direct observation in the X-ray is not common, so they continued to find candidates from other catalogues. These samples were pre-selected in other wavelengths with, again, a previously calculated $z > 4.5$. In particular, they looked at the NIR/MIR CANDELS catalogue and ALMA/SCUBA-2 detections in the CDF-S field. Cowie et al. (2020) Used the SED fitting program MAGPHYS described in Sec. 5 to help select from the ALMA catalog. In the end, they compiled a list of tens of candidates that had a previously calculated photometric redshift greater than 4.5.

As mentioned, it is not usually realistic to calculate a spectroscopic redshift for objects that are this far away. The problem with photometric redshift, however, is that it often has a large error, due to the statistical nature of a photometric redshift calculation. So, the next step for Cowie et al. (2020) was to recalculate the photometric z for all the objects in the FIR/submillimeter bands. They found that most of their candidates' previous estimates were far too high. The submillimeter band has a smaller associated error than previous measurements because it is a very thin band. In the end, their final candidate list contained only sources which had an estimated $z > 4.5$ in both the optical and the FIR/submillimeter. Ultimately, they found 11 $z > 4.5$ candidate sources to analyze, these are plotted in Fig. alongside some lower redshift sources from Barger et al. (2019). It should be noted that the errors on the final found redshifts are still rather large, once again due to the limitations in determining photometric redshift.

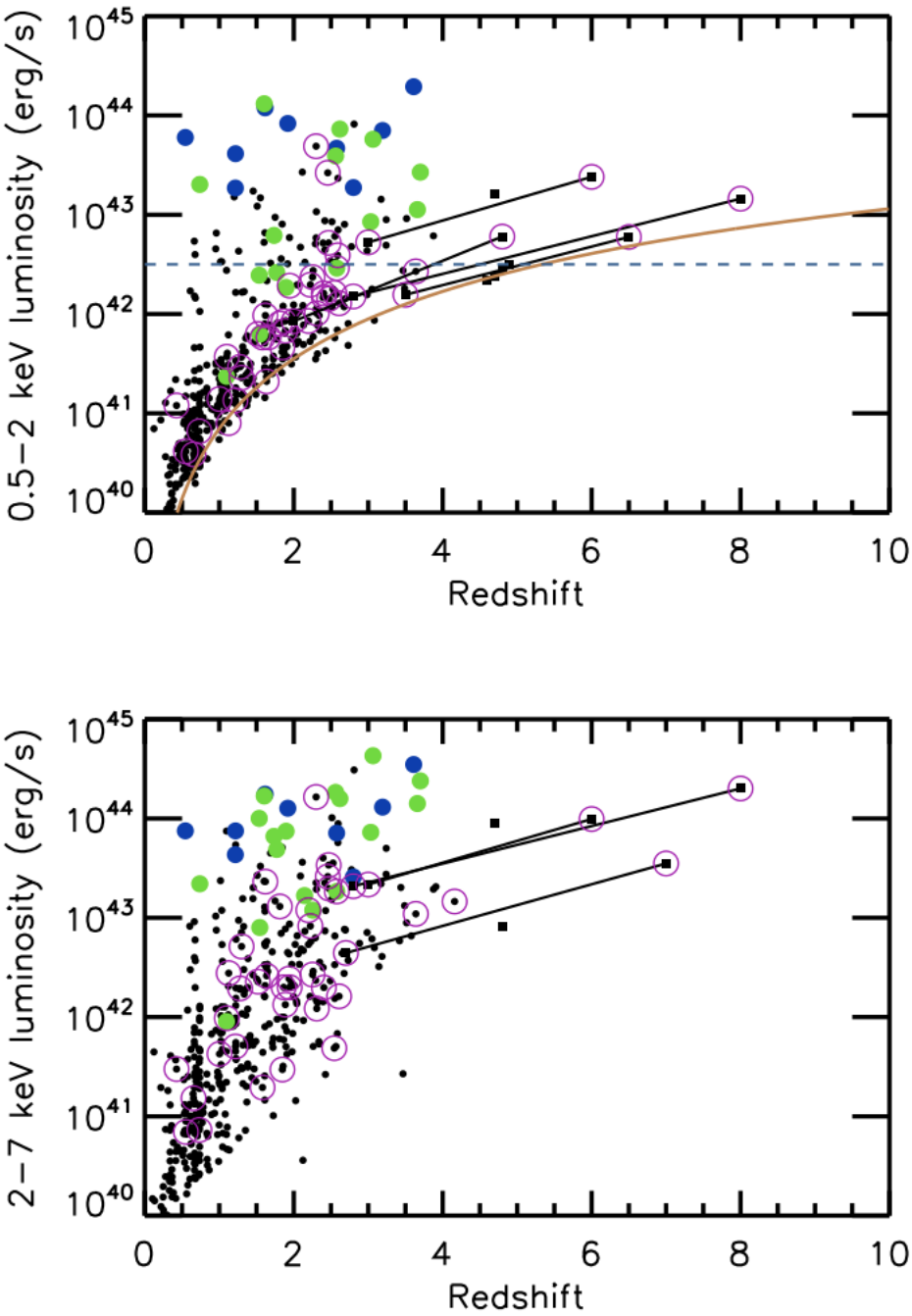

Figure 2. Luminosities (across two different energy bands) vs. Redshift for a number of AGN candidates. Blue dots are known broad-line AGNs, green dots are Seyfert type-2 galaxies. Purple circles are ALMA sources, connected by a black line in the case of sources with ambiguous redshifts.

4. RESULTS

Cowie et al. (2020) finds only 11 possible $z > 4.5$ AGN sources in the CDF-S. The primary result found that the number-density of AGN sources drops dramatically from redshift z=3 to z=6. From this, the primary conclusion was that there seems to have been very little black hole accretion during the time z=5-10, as expected. Cowie et al. (2020) also notes that the X-ray density from areas

corresponding to these redshifts is not high enough for the expected black hole mass gain during this time, further confirming this conclusion. Of the few high-redshift AGNs confirmed, the three highest are submillimeter and obscured X-ray sources. Two of these must be Compton-thick sources, similar to at least one previous source found in the $z \approx 4.8$ range (Gilli et al. 2011).

5. ANALYSIS

5.1. *Motivation and Introduction*

In Cowie et al. (2020), the final results find 11 $z > 4.5$ AGN candidates (see Tab.1). Just a small handful, given the number density expected to account for SMBH growth from $z = 5 - 10$. My goal is to further reconsider the type of galaxies these final candidates may be. If it turns out these candidates are not AGN galaxies, then the conclusions regarding AGN number density presented in Cowie et al. (2020) are further supported. It is possible for a regular galaxy (particularly a star-forming elliptical) to be mistaken for an AGN at a higher redshift. Additionally, galaxies at a very high redshift, like those studied in Cowie et al. (2020), will have notable morphological differences compared to nearby galaxies, making them all the more difficult to classify. One way to unravel this is to look at the spectral energy distributions (SEDs). The SED of a star-forming galaxy will take on a different general shape than that of an AGN (Polleta et al. 2007). In particular, a star-forming galaxy will have a dip in spectral energy at higher wavelengths compared to an AGN. This is because the different parts of an AGN's structure emit light at different wavelengths. In particular, the accretion disk of dust will emit strongly in the red. A star-forming galaxy, however, will have the majority of its spectral energy in the blue part of the spectrum, because the light emitted from star formation processes is higher energy. Therefore, an AGN SED will typically be more constant (flatter) than that of a star forming galaxy. Note that for this analysis, I will be referring to the different candidate galaxies by their ID number as seen in Table 4 of Cowie et al. (2020).

No.	RA(deg)	Dec(deg)	z
1	53.1971	-27.8279	4.5(4.2–4.9)
2	53.1411	-27.7644	4.6(4.0–4.9)
3	53.1082	-27.8251	4.7(4.6–4.8)
4	53.1116	-27.7678	4.7(4.5–4.9)
5	53.1199	-27.7430	2.0–4.8
6	53.1479	-27.8618	4.8(4.2–4.9)
7	53.0876	-27.7210	4.9(1.0–5.4)
8	–	–	3.5–6.5
9	53.0410	-27.8377	3.0–6.0
10	53.1088	-27.8690	2.7–7.0
11	53.1466	-27.8710	2.8–8.0

Table 1. A subset of the final candidate data found in Table 4 of Cowie et al. (2020). The RA and Dec come from the GOODS-S CANDLES catalogue described in Guo et al. (2013). The original table included other catalog names, measured fluxes, and calculated luminosities that were not needed for my extended analysis.

5.2. *Procedure*

In order to analyze the shapes of the SEDs for the AGN candidates, I first had to fit the SEDs to the data from Guo et al. (2013). The SED data for the galaxies in Guo et al. (2013) was all publicly available in the ViseR database associated with the paper. The SED data is given as photometric fluxes of the object through a number of given filters (see Fig. 3). Because these filters cover a wide range of the electromagnetic spectrum (from .1 to 10 microns), an energy correlation function can be created. An energy density plot can be made from the correlation function, giving an SED. Unfortunately, object 8 from Cowie et al. (2020) was not included in the GOODS-S CANDLES catalogue. In order to maintain consistency in the filters observed in, I decided to drop this candidate from further analysis. With the available data, I used a program called MAGPHYS to fit SED models. This program was used in Cowie et al. (2020), where they utilized SED modeling to help with ALMA pre-selection. The program takes in two ASCII files–one with information about the filters used and the other with the galaxies' redshifts and the flux data obtained from VisieR. From here, the program compares the data to a library of many model SEDs and determines a best fit. It finally outputs a file listing the best-fit parameters and various statistics (including χ^2), and a file with the data of the best-fit line. While the program comes with its own IDL for plotting the model, I decided to write up my own version in MATLAB, in order to have more flexibility in the scales of the axes, among other things. This code is modeled on the given IDL and can be found at the end of this document.

The plotted SED model fits can be compared to example SED shapes from Polleta et al. (2007) (See Fig. 4) to get a sense of what types of galaxies they may be. The Polleta et al. (2007) plots show star-forming galaxies in the left column, and two types of AGNs in the center and right hand columns. It should be noted that the known galaxies used to create the Polleta et al. (2007) SEDs are at lower redshift than the sources studied in Cowie et al. (2020). This is because, as discusses above, it is easier to classify galaxies at low redshift because their morphology is familiar. As discussed previously, a star-forming galaxy will have a drop in emission in redder wavelengths, while an AGN will remain more constant, because different types of emission coming from the AGNs various structures, particularly the accretion disk. Additionally, an analysis of the χ^2 statistic can yield more information about the galaxy type. Because the MAGPHYS program is trained on star-forming galaxies, AGNs are expected to have a worse fit (a higher χ^2 value).

5.3. *Results*

In order to get a better sense of what sort of galaxies are in this set, we can compare the sample SEDs from Polleta et al. (2007) in Fig. 4. Comparing this image to the model SEDs, it seems that a number of the candidates from Cowie et al. (2020) are AGN1 type galaxies, in line with the results of the paper. However, the χ^2 goodness-of-fit statistic for each model (see Tab.2) can help asses this conclusion. SED 3 is the one that appears most like the typical star-forming galaxy SEDs seen in Fig.4. The characteristic dip in energy with increased wavelength is apparent. In comparison, the AGN SEDs tend to stay more constant with respect to wavelength. In addition, model 3 has a relatively small χ^2 statistic, implying that the fit of the generated model is good for the data taken. Objects 5 and 9 have a unique shape that is higher at large wavelengths compared to the other models. Models 6 and 10 have relatively high χ^2 values. Because the MAGPHYS program is primarily trained on star formation SEDs, these high values imply a higher likelihood that these objects are, in fact, high-energy AGNs, like the AGN2s shown in the right hand column of Fig4.

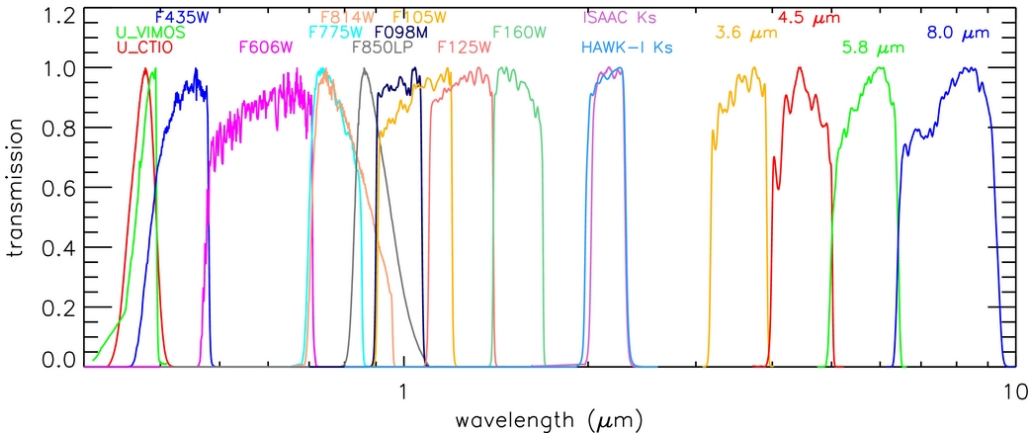

Figure 3. The different filters used by the CANDLES catalogue. MAGPHYS did not have the U_CTIO filter in its log, so the measurements in this filter were not included in the final fitting. Image from Guo et al. (2013).

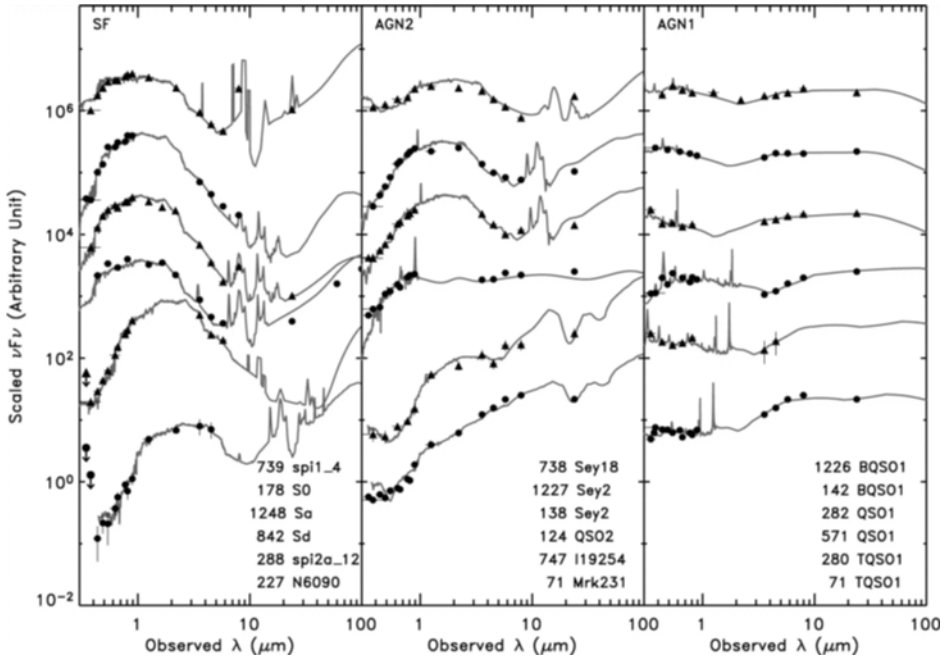

Figure 4. Best-fit SED model examples for three types of Galaxies. The left panel is star-forming galaxies, while both the center and right panels are types of AGN (AGN1 and AGN2, respectively). Image from Polleta et al. (2007).

Once again, in line with the results of Cowie et al. (2020). Objects 1,2, and 4 seem to be in a bit of a gray area, with shapes that could potentially be SF or AGN1 type galaxies. It is possible that these gray-area sources are Compton-thick, which would change the shape of the SED.

This analysis further supports the Cowie et al. (2020) conclusion that there is a significant drop-off in AGN number density at $z > 3$. Of the (already few) candidates found, it seems at least one of them (object 3, with $\chi^2 = 0.535$) is actually a star-forming galaxy. Several other candidates sit in a so-called "gray area," where their SED shapes and χ^2 statistics do not yield a clear classification. These candidates would need to be studied further. Some next steps toward investigating these

Object	χ^2
1	0.990
2	0.572
3	0.535
4	0.756
5	1.879
6	8.440
7	0.975
9	1.866
10	10.640
11	0.206

Table 2. The χ^2 goodness-of-fit results for the models generated by MAGPHYS

candidates could include measuring the strength of the OII and NIII spectral lines, and plotting them on a BPT diagram. This would have been done as part of the analysis of this paper, except that these lines will have been redshifted out of the visible spectrum, and no infrared spectrum was available.

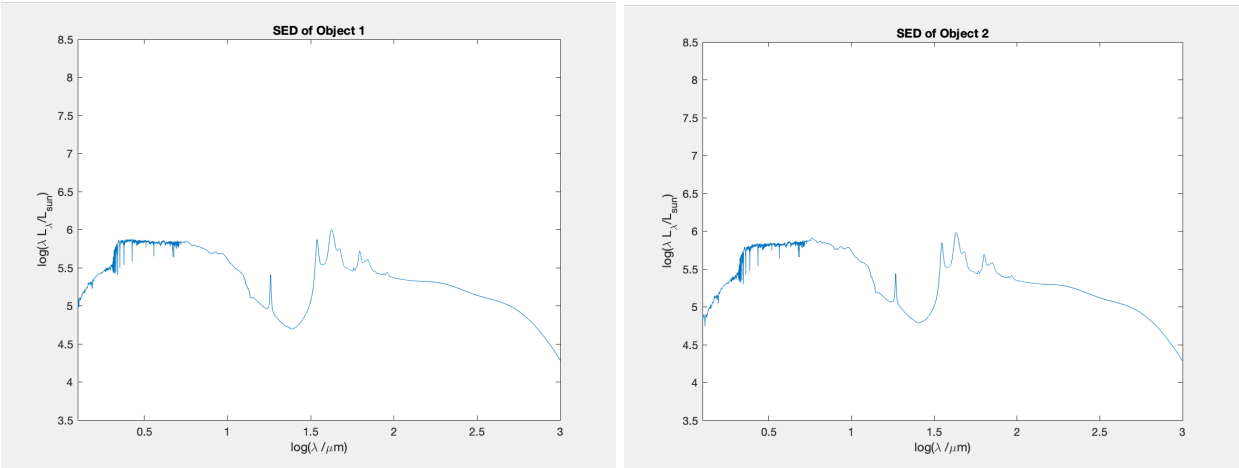

Figure 5. The final SED fits for each of the 10 galaxies in question. (Continued on next page).

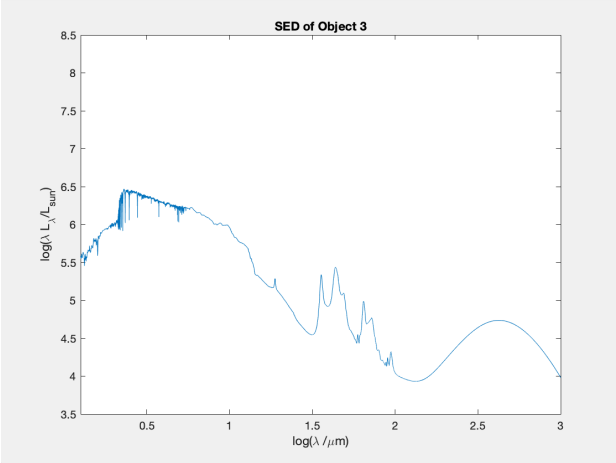
SED of Object 3
log(λ L_λ /L_sun)
log(λ /μm)

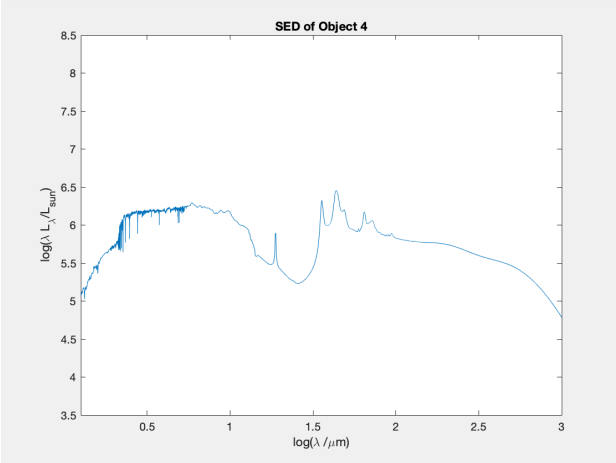
SED of Object 4
log(λ L_λ /L_sun)
log(λ /μm)

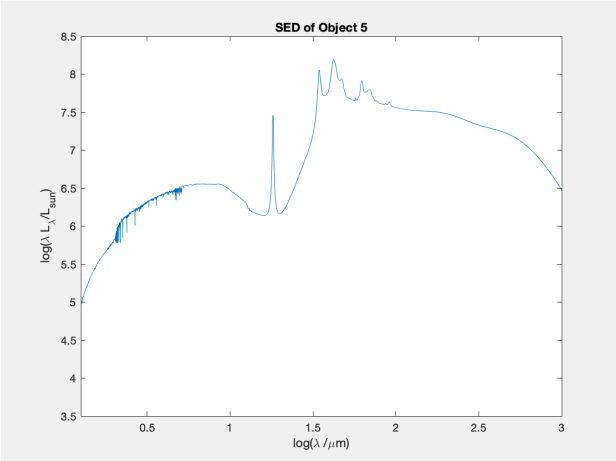
SED of Object 5
log(λ L_λ /L_sun)
log(λ /μm)

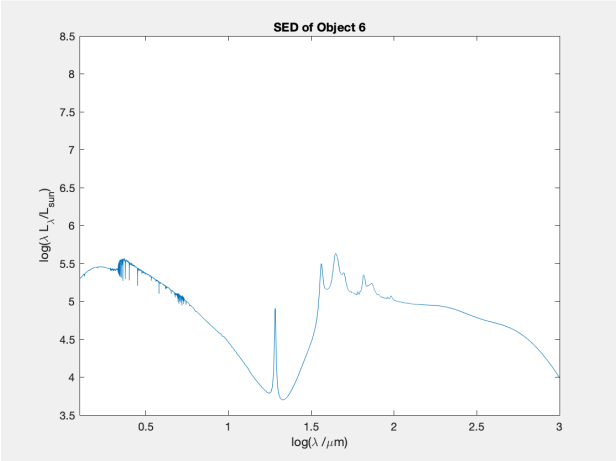
SED of Object 6
log(λ L_λ /L_sun)
log(λ /μm)

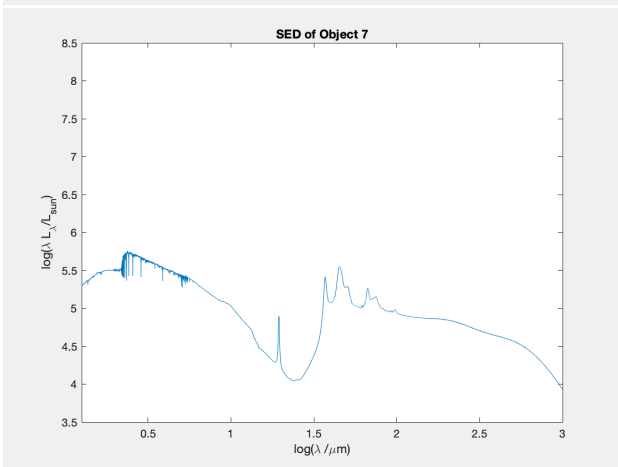
SED of Object 7
log(λ L_λ /L_sun)
log(λ /μm)

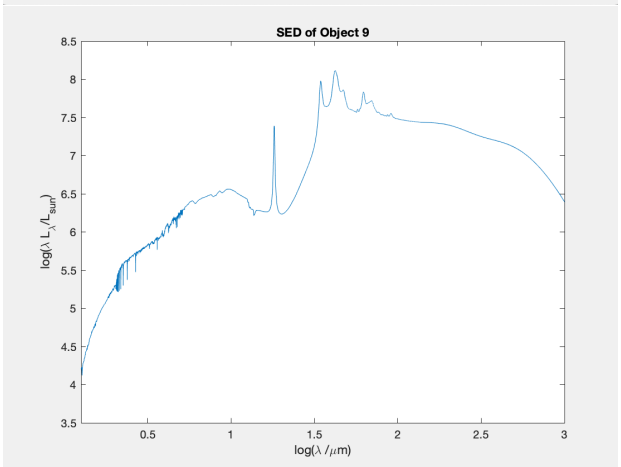
SED of Object 9
log(λ L_λ /L_sun)
log(λ /μm)

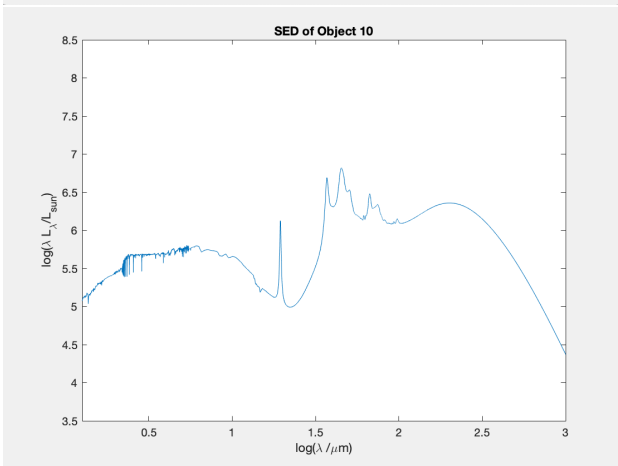
SED of Object 10
log(λ L_λ /L_sun)
log(λ /μm)

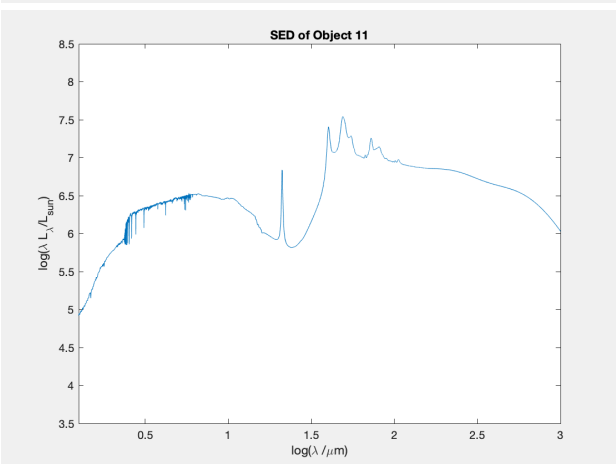
SED of Object 11
log(λ L_λ /L_sun)
log(λ /μm)

REFERENCES

L. L. Cowie, A. J. Barger, F. E. Bauer, et al. 2020, ApJ (accepted for publication)

Barger, A. J., Cowie, L. L., Bauer, F. E., and González-López, J. 2019, ApJ, 887, 23

Gilli, R., Su, J., Norman, C., et al. 2011, ApJ, 730, L28

Y. Guo, H. C. Ferguson, M.Giavalisco, et al. 2013, ApJS, 207, 24

M. Polletta, M. Tajer, L. Maraschi, et al. 2007, ApJ, 663, 81-102